Chemical Geology 525 (2019) 356–367

Contents lists available at ScienceDirect

Chemical Geology

journal homepage: www.elsevier.com/locate/chemgeo

U-Pb memory behavior in Chicxulub's peak ring — Applying U-Pb depth profiling to shocked zircon

Cornelia Rasmussen[a,*], Daniel F. Stockli[a], Catherine H. Ross[a], Annemarie Pickersgill[b,c], Sean P. Gulick[a], Martin Schmieder[d], Gail L. Christeson[a], Axel Wittmann[e], David A. Kring[d], Joanna V. Morgan[f], and the IODP-ICDP Expedition 364 Science Party

[a] Institute for Geophysics and Department of Geological Sciences, Jackson School of Geosciences, University of Texas at Austin, Austin, TX, USA
[b] School of Geographical and Earth Sciences, University of Glasgow, Glasgow, UK
[c] Argon Isotope Facility, Scottish Universities Environmental Research Centre (SUERC), East Kilbride, UK
[d] Center for Lunar Science and Exploration, Universities Space Research Association Lunar and Planetary Institute, Houston, TX, USA
[e] Eyring Materials Center, Arizona State University, Tempe, AZ, USA
[f] Department of Earth Science and Engineering, Imperial College London, SW7 2AZ, UK

ARTICLE INFO

Editor: Balz Kamber

Keywords:
Chicxulub
U-Pb systematics
LA-ICP-MS depth profiling
Metamictization
IODP

ABSTRACT

The zircon U-Pb system is one of the most robust geochronometers, but during an impact event individual crystals can be affected differently by the passage of the shock wave and impact generated heat. Unraveling the potentially complex thermal history recorded by zircon crystals that experienced variable levels of shock and heating, as well as additioanl pre- and post-impact thermal events, has been difficult using classical geochronological methods. The existing high-precision $^{40}Ar/^{39}Ar$ age constraints for the K-Pg Chicxulub event, and the previous U-Pb dating of the basement rocks from the impact site, make Chicxulub an ideal location to study impact-induced effects on the zircon U-Pb systematics and to evaluate potential 'memory effects' of pre-impact U-Pb signatures preserved within those individual zircon crystals. Recent IODP-ICDP drilling of the Chicxulub impact structure recovered 580 m of uplifted shocked granitoid and 130 m of melt and suevite, providing an unprecedented opportunity to study zircon crystals subjected to a range of shock pressures, thermal, and deformational histories. Zircon morphologies were classified using scanning electron microscopy (SEM) imaging and then samples were depth profiled using laser ablation inductively coupled plasma mass-spectrometry (LA-ICP-MS) to document the range of preserved age domains from rim-to-center within individual crystals. The results show U-Pb ages range from 66 to 472 Ma, which are consistent with both inherited Carboniferous and Late Paleozoic basement ages as well as Pb loss ages in response to the K-Pg impact event. While the bulk of the zircon grains preserve Paleozoic ages, high U (metamict) zones within fractured zircon crystals exhibited an age within uncertainty (66 ± 6.2 Ma) of the impact age (66.038 ± 0.049 Ma), indicating that inherited intragrain U-Pb kinetics and/or hydrothermal fluid flow may have controlled age resetting those zircon crystals rather than impact-induced shock and heating alone. Moreover, the calculated α-decay doses suggest that the zircon crystals experienced Stage 1 or early Stage 2 radiation damage accumulation. Therefore, we suggest that the lowered crystal annealing temperature in crystals that previoulsy experienced radiation damage make the zircon U-Pb clock either more susceptible to the relatively short heat pulse of the impact event, the moderate pressure and temperature conditions in the peak ring, and/or to hot-fluid flow in the long-lasting post impact hydrothermal system.

1. Introduction

Hypervelocity impact events have played a key role in solar system evolution by extensively resurfacing planetary bodies and altering the course of life on Earth, in case of the Chicxulub impact event, by causing a mass extinction and dramatic short- and long-term environmental changes (e.g., Alvarez et al., 1980; Melosh, 1989; Hildebrand et al., 1991; Farmer, 2000; Kring, 2007). In order to evaluate the role of impacts in Earth's history, it is crucial to accurately determine the ages of impact events and to understand the impact-induced alteration of

* Corresponding author.
E-mail address: crasmussen@utexas.edu (C. Rasmussen).

https://doi.org/10.1016/j.chemgeo.2019.07.029
Received 29 December 2018; Received in revised form 20 July 2019; Accepted 24 July 2019
Available online 27 July 2019

materials suitable for age determination (e.g., Deutsch and Schärer, 1994; Jourdan et al., 2009, 2012; Jourdan, 2012). Only with robust high-resolution chronology will we be able to answer fundamental questions about impact-induced environmental change, extinction events, and the impact cratering flux through geologic time (e.g., French, 1998; Bland, 2005; Schulte et al., 2010). Further, inherited target rock ages obtained from target rocks and impactities can hold fundamental information about the pre-impact thermal history of the target area including the identification of previous unknown target materials, evaluating the origin of impactites, times of high impact flux, and the cratering process itself (e.g., Compston et al., 1987; Krogh et al., 1993a, 1993b; Abbott et al., 2012; Petrus et al., 2016).

The U-Pb and $^{40}Ar/^{39}Ar$ systems are regarded as high-precision chronometers and the backbones for the calibration of the geologic time scale (Gradstein, 2012). Both radioisotopic clocks, however, are susceptible to partial age resetting combined with open system behavior and additional diffusion of their daughter products in post-impact time (e.g., Deutsch and Schärer, 1994; Jourdan et al., 2009). Shocked zircon, most commonly used for U-Pb geochronology, exhibits impact-induced, (partial) open-system behavior and recrystallization due to shock metamorphism (e.g., Krogh et al., 1993a, 1993b; Wittmann et al., 2006; Timms et al., 2017). Zircon shock features, such as fracturing (irregular or planar), deformation twinning, the transformation to reidite, or the recrystallization to granular zircon might introduce additional diffusion pathways hampering with the age preservation of the zircon U-Pb clock (Wittmann et al., 2006; Schmieder et al., 2015; Schmieder et al., 2018; Timms et al., 2017; Kenny et al., 2019). This is complicated further by the fact that zircon crystals are able to also preserve partial age information of the time of crystallization as well as of pre- and post-impact thermal events (e.g., Mezger and Krogstad, 1997; Petrus et al., 2016). This behavior results in a wide range of recovered ages associated with pre-impact, impact, and/or post-impact processes that do not necessarily reflect the time of impact and that are often characterized by a high degree of discordance (e.g., Krogh et al., 1993a, 1993b; Deutsch and Schärer, 1994; Kamo and Krogh, 1995).

However, individual zircon crystals have the potential to capture and retain information about multiple thermal events, including the impact age, within a single crystal and thus might be able to resolve the thermal history of an impact crater (Mezger and Krogstad, 1997; Petrus et al., 2016). The challenge, however, is to identify those different age domains and unlock that information. The presence of different age domains within a single zircon crystal represents a challenge for traditional U-Pb techniques in which either the entire crystal is dissolved, such as in isotope dissolution thermal ionization mass spectrometry (ID-TIMS), or where polished minerals are analyzed using spot techniques, such as in laser ablation inductively coupled plasma mass spectrometry (LA-ICP-MS), secondary ion mass spectrometry (SIMS), or sensitive high resolution ion microprobe (SHRIMP) analysis.

LA-ICP-MS depth profiling has previously been applied to complex metamorphic zircon populations (Kelly et al., 2014; Marsh and Stockli, 2015). For example, Marsh and Stockli (2015) determined ages and trace element compositions of zircon rims and interior domains in granulites from the Grenville Province, Canada. U-Pb depth profiling may also be a powerful tool in impact crater geochronology and geochemical analyses when applied to terrestrial impact crater lithologies. Here we apply this technique, for the first time, to shocked zircon crystals extracted from granitoid and melt rocks of the Chicxulub peak ring.

We obtained core samples from the International Ocean Discovery Program (IODP)-International Continental scientific Drilling Program (ICDP) Expedition 364 that drilled Chicxulub's peak ring (Fig. 1A) on the Yucatán Peninsula in 2016. The ages of the impact (66.038 ± 0.049 Ma, Renne et al., 2013; Sprain et al., 2018) and that of the target rock (~550–300 Ma, Kettrup and Deutsch, 2003; Xiao et al., 2017) are relatively well constrained. U-Pb depth profiling of zircon from Chicxulub therefore represents an excellent case study to identify which age domains are preserved in this setting and what controls the age preservation related to pre-impact alteration (e.g., regional tectono-thermal events, radiation damage), impact heating, levels of shock, or post-impact hydrothermal fluid flow.

After describing the crystal morphology of zircon extracted from shocked granitoid peak ring lithologies and impactite samples using scanning electron microscopy (SEM), we employed LA-ICP-MS depth profiling and one-second depth increment analysis to characterize the spatial distribution of preserved age domains and trace element concentrations (here U and Th [ppm]) within individual zircon crystals. These different age domains were used to elucidate the complex alteration histories within partly reset zircon age populations.

2. Geological setting

The ~200 km wide Chicxulub impact structure represents one of the largest known impact craters on Earth (Hildebrand et al., 1991; Morgan et al., 1997). The crystalline basement of the Yucatán Peninsula, and therefore the lower portion of the target rock of the Chicxulub impact event, experienced pre-impact thermal alteration due to regional tectonism, leading to a complex radioisotopic age inventory (Krogh et al., 1993a, 1993b; Kamo et al., 2011; Kettrup and Deutsch, 2003, and references therein; Xiao et al., 2017).

Krogh et al. (1993a) reported a Concordia upper intercept U-Pb TIMS age of 545–572 Ma from shocked zircon crystals from Chicxulub ejecta deposits, which corresponds to the pan-African orogeny (750–530 Ma; Lopez et al., 2001; see also: Krogh et al., 1993b; Premo and Izett, 1993; Kamo and Krogh, 1995; Keppie et al., 2011; Schmieder et al., 2018). In addition, other upper intercept ages of ~418 Ma have been reported and linked to Silurian plutonic intrusions in the Maya Mountains of the Yucatán (see also Bateson, 1972; Steiner and Walker, 1996). Xiao et al. (2017) reported preliminary LA-ICP-MS U-Pb ages from the IODP Exp. 364 core, ranging from ~300 to 340 Ma, which they interpreted as the products of protracted Carboniferous magmatism. Those ages are in agreement with a LA-ICP-MS U–Pb age of 341 ± 6 Ma for magmatic titanite in granitoid rock from the Chicxulub peak ring (Schmieder et al., 2017). Triassic and Jurassic dike emplacement, associated with the opening of the Gulf of Mexico, has also been reported for the Yucatan basement on the basis of K-Ar ages of 230 Ma (cf., Steiner and Walker, 1996) and intrusion ages of ~190–160 Ma from DSDP core (Leg 77) in the southeastern Gulf of Mexico (Schlager et al., 1984).

IODP-ICDP Expedition 364 (Hole M0077A; 21.45°N, 89.95°W) recovered an 829-m-long continuous core section (505.7–1334.7 m below sea floor [mbsf]), composed of (bottom to top): (i) 586.7 m (748–1334.7 mbsf) of coarse-grained granitoid basement that is traversed by both pre-impact and impact-generated dykes; (ii) 130 m (618–748 mbsf) of impactites (clast-poor melt sheet topped by suevite or melt-bearing polymict impact breccia); and (iii) 113 m (505–618 mbsf) of Paleogene sediments (Morgan et al., 2016). The peak ring mainly consists out of granitic basement rocks that were uplifted ~8–10 km during crater formation (Morgan et al., 2016) (Fig. 1B). The granitoid basement section displays impact-induced deformation including fractures, shear zones, and cataclasites (Riller et al., 2018), post-impact high- and low temperature hydrothermal mineral alteration (Kring et al., 2017a, 2017b; Schmieder et al., 2017), and shock metamorphic features (e.g., planar deformation features, planar fractures, and feather features in quartz) (Gulick et al., 2017a), indicative of shock pressures of ~12–17 GPa (Rae et al., 2017).

3. Material and methods

For this study, we carried out U-Pb LA-ICP-MS depth profiling on zircon crystals extracted from five core samples (sample name: rock type-mbsf-crystal number) from the shocked granitoid rock (G-) (sample IDs: G-875mbsf-1; G-1090-1; G-1310-1/-2; and G-1330-1) (5

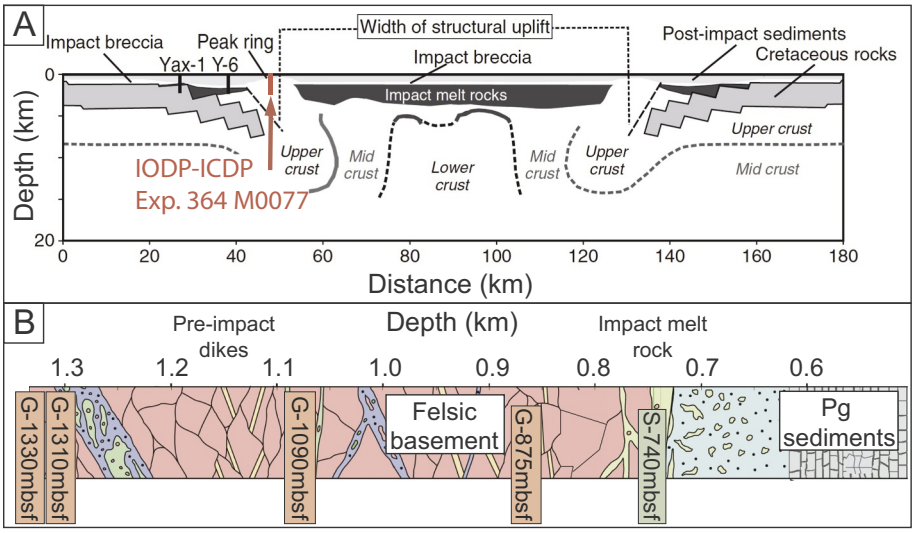

Fig. 1. Geological setting. (A) Cross-section of the Chicxulub impact structure showing the location of the IODP Exp. 364 drilling (red line) (after Gulick et al., 2013, after Vermeesch and Morgan, 2008). (B) Stratigraphic section of the drill core recovered by IODP Exp. 364 (modified from Morgan et al., 2016) with sample locations for this study indicated. (For interpretation of the references to color in this figure legend, the reader is referred to the web version of this article.)

Table 1
Summary of sample information and all $^{206}Pb/^{238}U$ weighed mean ages including their uncertainties, obtained from the individual depth profiles, as well as the associated U and Th [ppm] concentrations and calculated α-decay damage [α/mg]. (ZM = zircon morphology).

Crystal ID	Core ID	MBSF	ZM	Plateau Ages	Age ± 2σ	MSWD	U (ppm)	U (ppm) ± 2σ	Th (ppm)	Th (ppm) ± 2σ	α decay dose [α/mg]	α decay dose ± 2σ
S-740mbsf-1	93-R-1-1	740	4	412	5.4	1.30	274	10	331	19	5.06E+14	2.59E+13
S-740mbsf-2A	93-R-1-2a	740	4	140	2.9	1.40	308	6	298	13	1.78E+14	8.39E+12
S-740mbsf-2A	93-R-1-2a	740	4	228	4.8	0.03	102	4	86	7	9.49E+13	5.28E+12
S-740mbsf-2B	93-R-1-2b	740	4	88	5.9	1.80	299	9	309	15	1.11E+14	7.13E+12
S-740mbsf-2B	93-R-1-2b	740	4	169	6.1	0.23	182	6	189	12	1.43E+14	1.23E+13
S-740mbsf-2B	93-R-1-2b	740	4	104	2.5	1.16	93	4	85	6	3.88E+13	3.61E+12
S-740mbsf-3A	93-R-1-3a	740	3	350	11.0	1.40	357	49	155	20	4.68E+14	8.08E+13
S-740mbsf-3A	93-R-1-3a	740	3	447	5.5	0.93	1236	28	632	27	2.09E+15	6.82E+13
S-740mbsf-3A	93-R-1-3a	740	3	392	3.2	1.40	840	15	972	25	1.41E+15	3.02E+13
S-740mbsf-3B	93-R-1-3b	740	3	472	4.4	1.60	1098	39	786	25	2.06E+15	7.31E+13
S-740mbsf-3B	93-R-1-3b	740	3	383	2.4	0.59	575	21	658	28	9.45E+14	3.62E+13
S-740mbsf-4	93-R-1-4	740	1	298	2.0	1.19	127	5	116	9	1.54E+14	9.34E+12
G-875mbsf-1	145-R-3-1	875	2	284	6.5	1.10	1003	103	415	73	1.07E+15	9.16E+13
G-875mbsf-2	145-R-3-1	875	2	171	4.3	0.98	3391	154	3690	172	1.54E+15	1.53E+14
G-875mbsf-3	145-R-3-1	875	2	293	4.3	1.19	676	31	372	30	7.55E+14	2.9E+13
G-1090mbsf-1	224-R-1-1	1090	2	88	3.1	1.90	9763	628	12,925	820	3.78E+15	2.03E+14
G-1090mbsf-2	224-R-1-1	1090	2	66	6.2	7.00	7857	477	11,487	507	2.41E+15	1.21E+14
G-1310mbsf-1	296-R-1-1	1310	1	328	2.4	0.83	566	20	506	25	7.53E+14	3.39E+13
G-1310mbsf-2	296-R-1-2	1310	2	86	5.0	2.80	9202	1605	5908	482	2.75E+15	2.88E+14
G-1310mbsf-2	296-R-1-2	1310	2	175	9.3	1.40	2163	142	1932	167	1.56E+15	8.80E+13
G-1310mbsf-2	296-R-1-2	1310	2	80	3	2.10	3886	174	2828	220	1.21E+15	7.15E+13
G-1330mbsf-1	302-R-1-1	1330	2	311	5.4	0.33	1585	165	769	54	1.84E+15	1.69E+14

crystals) and from one sample of impact melt rock (M-) (sample ID: M-740mbsf-1/-2/-3) (3 crystals) (Table 1). A detailed rock description can be found in the Expedition 364 Preliminary Report (Gulick et al., 2017b). All samples underwent standard mineral separation, including jaw- and hand-crushing, Wilfley table, magnetic separation with a hand magnet, and methylene iodide heavy liquid separation. The separated zircon crystals were hand-picked and mounted under a binocular microscope onto double-sided adhesive tape on one-inch diameter acrylic discs.

Prior to LA-ICP-MS analyses, the zircon crystals were imaged using SEM to characterize the crystal morphology using a JEOL 6490LV SEM in low-vacuum mode and without carbon coating at the University of Texas at Austin Electron Microbeam Laboratories. All depth-profile LA-ICP-MS analyses were conducted at the University of Texas at Austin at the (U-Th)/He and U-Pb Geo-Thermochronometry Laboratory using a Photon Machines 193 nm Analyte G2 excimer laser-ablation system with large-volume Helex sample cell, coupled to a Thermo Scientific Element2 HR-ICP-MS. Due to the relatively small zircon crystal sizes, a spot size of 25 μm was chosen and an ablation time of 30 s (40 s for crystals of sample M-740 mbsf). Each crystal was depth-profiled by continuous analysis to a laser pit depth of 15 or 20 μm (ablation rate ~0.5 μm/s). The experimental settings were: laser energy of 4 mJ, laser frequency of 10 Hz, and a gas flow of 0.475 L (line 1) and 0.225 L (line 2) respectively. The analyses of unknowns were conducted against an interspersed primary zircon standard (GJ-1, 601.7 ± 1.3 Ma; Jackson et al., 2004) and two secondary procedural standards (Plešovice, 337.1 Ma; Sláma et al., 2008 and Pak1, 43.03 ± 0.01 Ma, UT in-house) (Fig. S1).

Data reduction was conducted using the IgorPro (Paton et al., 2011) based Iolite software with VizualAge data reduction scheme (Iolite version: 3.6; Geochron DRS: Visual age) (Petrus and Kamber, 2012). The data were corrected for both downhole and mass fractionation (Fig. S2) and exported as one-second increments to identify different age domains from depth profiles of the individual zircons. A ^{207}Pb-based initial common Pb correction, using a Stacey and Kramers (1975) crustal common Pb evolution model, was applied to each one-second increment by using the initial Pb isotopic composition calculated from the estimated U-Pb ages of the sample (e.g., Andersen, 2002). The

Isoplot/Ex.4.15 program (Ludwig, 2008) was used to display the results both as Wetherill concordia diagrams (Wetherill, 1956), Tera-Wasserburg concordia diagrams (Fig. S3), and age spectra to visualize variations in age with increasing ablation depth/time.

While we report all data, our age domain interpretations are based on the corrected $^{206}Pb/^{238}U$ ages since these two isotopes were directly measured during the LA-ICP-MS analyses and due to the counting-statistical imprecision associated with the $^{207}Pb/^{235}U$ measurements, especially in crystals < 400 Ma (Spencer et al., 2016). Data were filtered for laser ablation penetration through entire crystals, which is typically associated with: (1) a drop in the U (and Th) concentration; (2) no more obtainable ages; and/or (3) relatively high uncertainties (± > 100%). Data with these trends were removed from the data set.

Finally, we calculated the α-decay dose (Murakami et al., 1991) for individual one-second increments, (the used U and Th [ppm] concentrations are calculated based on primary standard GJ1) by:

$$D = 8\,N_1[\exp(a_1 t) - 1] + 7\,N_2[\exp(a_2 t) - 1] + 6\,N_3[\exp(a_3 t) - 1] \quad (1)$$

where N_1, N_2, N_3 represent ^{238}U, ^{235}U, and ^{232}Th respectively (atoms/mg); a equals the decay constants for each parent isotope (years^{-1}); and t is the age of the zircon from each decay chain. N_2 is assumed to be: $N_2 = (1/139)\,N_1$; based on natural abundance (also see Murakami et al., 1991).

4. Results

4.1. Crystal morphology

The exterior morphology and texture of the zircon crystals are described based on the following classification: (1) virtually undisturbed (zircon morphology (ZM) = 1); (2) irregularly fractured (ZM = 2); (3) planar fracturing (ZM = 3); and (4) granular texture (ZM = 4) (compare scheme of Schmieder et al., 2015). Two crystals are described as virtually undisturbed (M-740mbsf-4, G-1310mbsf-1; Fig. 2A). Four crystals display irregular fracturing (G-875mbsf-1, G-1090mbsf-1, G-1310mbsf-2, G-1330mbsf-1; Fig. 2B). One crystal shows possible planar fractures (M-740mbsf-3, Fig. 2C/D). Two crystals display a granular texture (M-740mbsf-1/-2; Fig. 2E/F) (Table 1). We acknowledge, however, that without a more detailed petrographic and microstructural description of the mineral interior (e.g., by cathodoluminescence (CL-) imaging or electron backscatter diffraction (EBSD) mapping), we are not able to reliably quantify the extent of internal structural damage within the zircon crystals. Rather, the described exterior zircon morphology can serve as a first-order indicator.

4.2. U-Pb depth profiling

The depth profiles reveal three main patterns that occur with variable distinctness: (a) age domains that display relatively little variability independent of ablation depth (M-740mbsf-4; G-1310mbsf-1); (b) age domains that become older with increasing ablation depth (younger rim ages, older interior ages) (M-740mbsf-1/-2A/-3A; G-1310mbsf-2); and (c) age domains that start out older and become younger with increasing ablation depth (older rims, younger interior domains) (M-740mbsf-2B/-3B; G-875mbsf-1; G-1090mbsf-1; G-1330mbsf-1).

Based on the one-second increment depth-profile data, internal domain ages within individual zircon crystals were determined on the basis of well-developed "age plateaus". Depth-profiling plateau ages were defined as a minimum of three continuous steps that overlap at 2-sigma uncertainty (including chi-squared distribution). The plateau ages were calculated as weighted mean ages (Ludwig, 2008). A summary of all the weighted mean ages, including their uncertainties, MSWD values, and trace element concentrations (U and Th [ppm]) can be found in Table 1 and in Figs. 3–6 (see also Table S1 for one-second increment isotope data).

Picking age plateaus, based on one-second increments can become subjective, in particular when dealing with zircon crystals that display an increase in alteration, exhibited by an increase in data scatter (Fig. 4, 5A–C). Therefore, weighted mean plateau ages were calculated based on data points that overlapped within 2-sigma with all other contiguous data points in the plateau.

Not all weighted mean ages display the same statistical robustness. For example, the second age plateau picked in analyses from sample M-740mbsf-2A (228 ± 4.8 Ma) is associated with a very low MSWD of

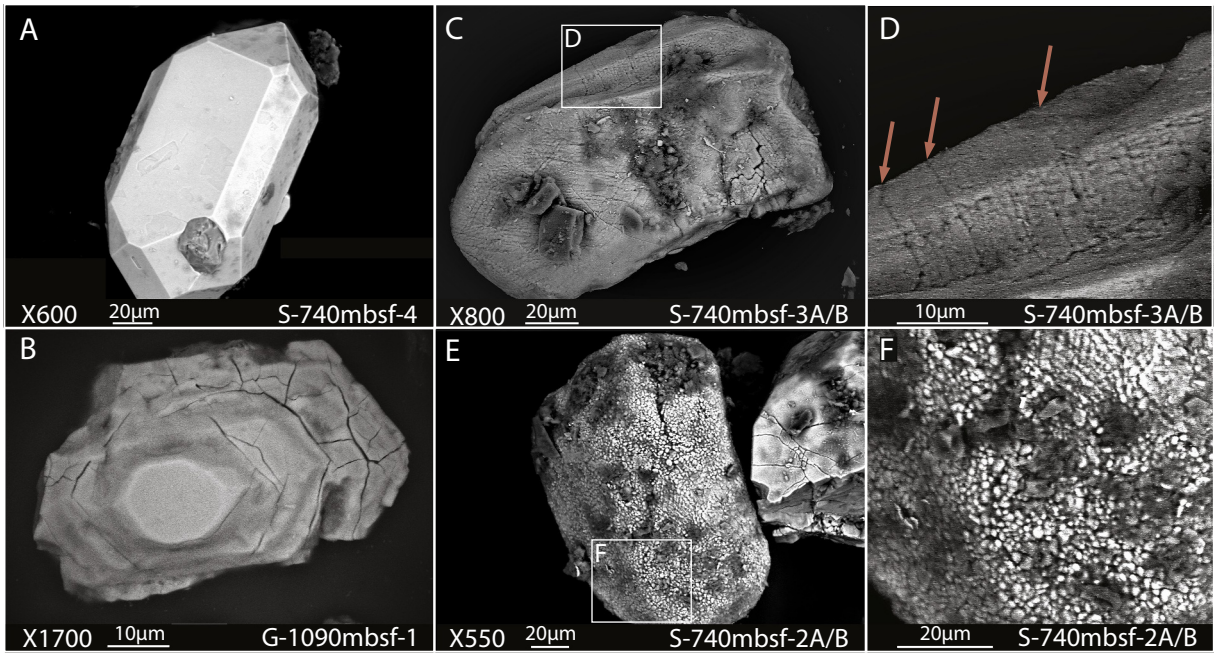

Fig. 2. Zircon morphology (ZM). (A) Virtually undisturbed (ZM = 1); (B) Irregular fractured (ZM = 2); (C) light fracturing in lower right corner and potentially planar fracturing (ZM = 3), (D) Close up of zircon crystal shown in (C); (E) zircon displaying granular textures (ZM = 4); and (F) Close up of zircon crystal shown in (E).

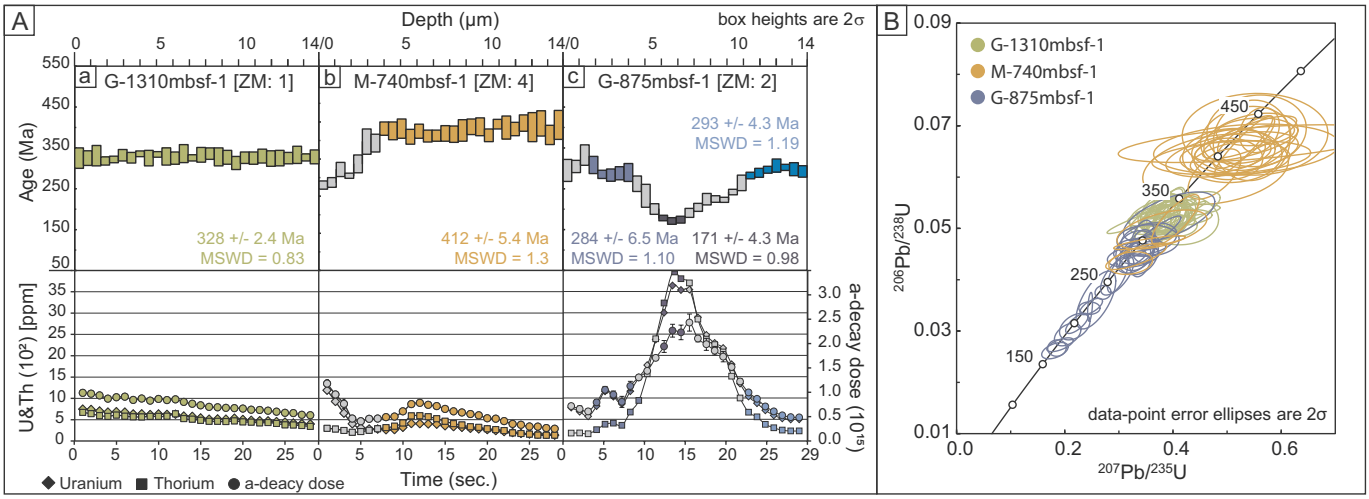

Fig. 3. U-Pb depth profiling: (A) U-Pb depth profiling including the calculated $^{206}Pb/^{238}U$ weighted mean ages for the respective zircon crystal (upper panels) (Individual boxes represent one-second increments within a single analysis, 2-sigma) vs. U and Th [ppm] concentrations as well as α-decay [α/mg] damage accumulation (lower panels). Three main patterns are observed: (A.a.) Relatively "closed system"; (A.b.) Younger rim and older interior ages; and (A.c.) Older rims and younger interior zones. The age spectra display $^{206}Pb/^{238}U$ age domains and U and Th [ppm] versus depth after downhole and mass fractionation correction. (ZM = zircon morphology). Pit ablation depth estimated based on previous laboratory calibration measurements using a Bruker Optical Profilometer. (B) Wetherill Concordia plot (1956) for each individual, complete, analyses (30/40 s). (Tera Wasserburg diagrams are visualized in Fig. S3).

0.03 (Fig. 5A). This mean age was derived from an age domain that appears to begin within the last 4 sof the analysis and possibly continues deeper within the crystal, therefore the MSWD is based on a low number of data points. A MSWD value of 0.03 is considered acceptable for a sample size of 4, based on the chi-squared distribution (Spencer et al., 2016). However, that age should only be considered preliminary. In contrast, for two plateaus the MSWD of the weighted mean lies outside the acceptable limits as suggested by Wendt and Carl (1991) and Spencer et al. (2016) (G-1090mbsf-1; G-1310mbsf-2) (Fig. 4). In both cases (two weighted mean ages), the relatively young ages of 66 ± 6.2 Ma (MSWD = 7.0, G-1090mbsf-1) and 80 ± 3.0 Ma (MSWD = 2.1, G-1310mbsf-2) are linked to increased U and Th concentrations. These domainal ages are less robust than the other ages, since the high MSWD suggests either over-dispersion of data or underestimation of uncertainties (Spencer et al., 2016). Some authors (e.g., Ludwig, 2008; Horstwood et al., 2016) account for high MSWD values by inflating the uncertainty of each weighted mean age by multiplying the standard error of the mean by the square root of the MSWD. If we apply this approach, then the above two ages become 66 ± 16 Ma (G-1090mbsf-1) and 81 ± 4.3 Ma (G-1310mbsf-2). Further, we observe that younger age domains are not necessarily solely located within the zircon rims, but also within interior domains of the zircon, which are also characterized by relatively elevated U and Th concentrations (M-740mbsf-3B; G-875mbsf-1; G-1090mbsf-1) (Figs. 3Ac, 4 Aa, 5B).

4.3. Trace element concentrations

In general, the trace element concentrations decrease with increasing ablation depth (see also Section 5.1. Quality of data). The

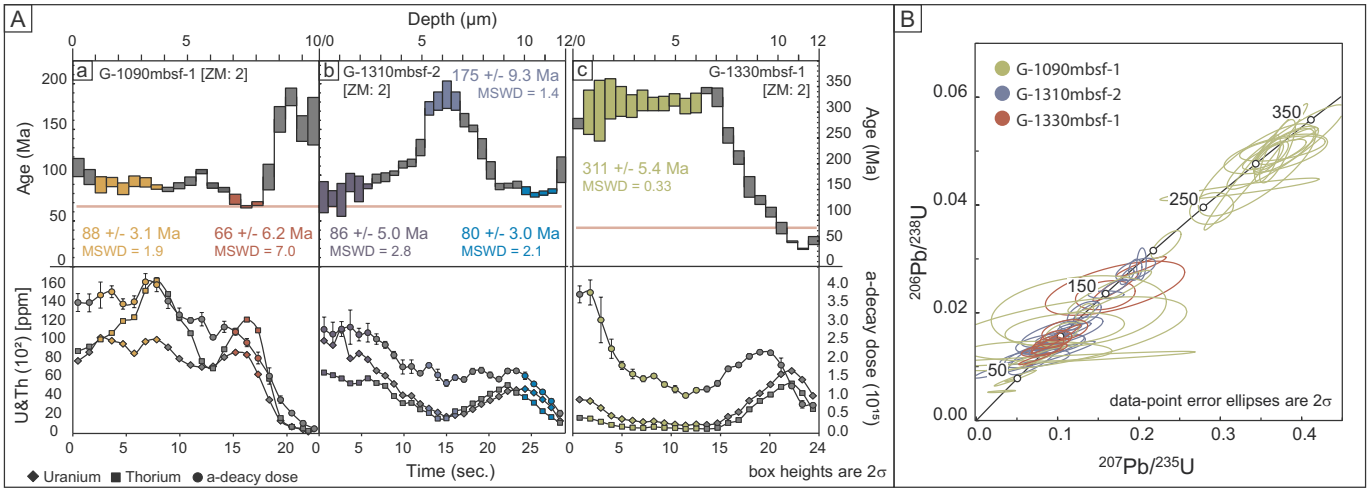

Fig. 4. (A) Increased alteration observed in $^{206}Pb/^{238}U$ depth profiles, apparent by increased data scatter and relatively high U and Th [ppm] concentrations and increased α-decay [α/mg] damage. (a-c) Red lines represent the impact age (66 Ma, Renne et al., 2013). Individual boxes represent one-second increments within a single analysis, 2-sigma. The age spectra display $^{206}Pb/^{238}U$ age domains and U and Th [ppm] versus depth after downhole and mass fractionation correction. (ZM = zircon morphology). Pit ablation depth estimated based on laboratory calibration measurements using a Bruker Optical Profilometer. (B) Wetherill Concordia plot (1956) for each individual, complete, analyses (30/40 s). (Tera Wasserburg diagrams are visualized in Fig. S3). (For interpretation of the references to color in this figure legend, the reader is referred to the web version of this article.)

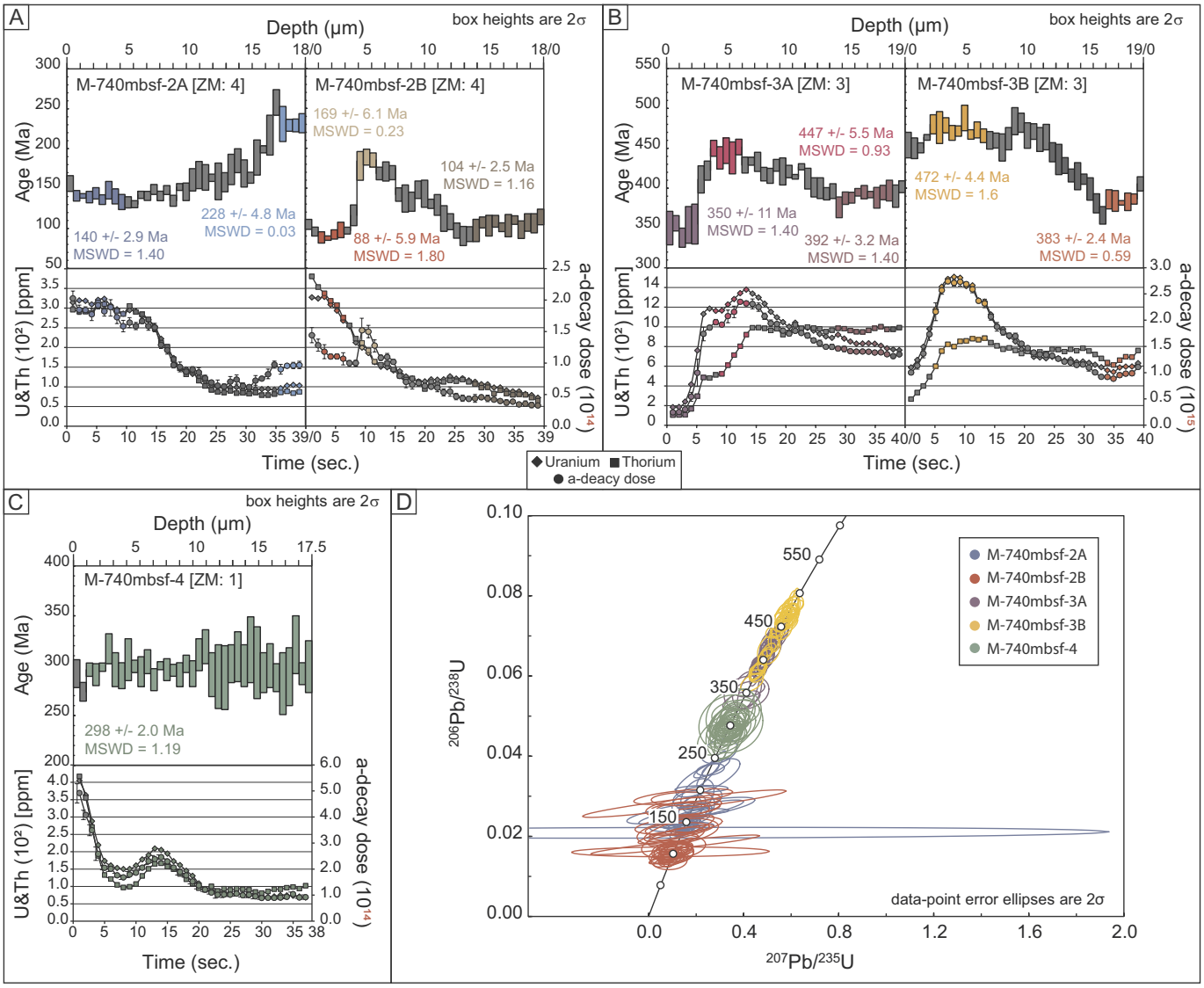

Fig. 5. U-Pb depth profiling of zircon including the calculated $^{206}Pb/^{238}U$ integration ages, extracted from the melt rock sample S-740mbsf ([A-C]; upper panels), vs. U and Th [ppm] concentrations and α-decay [α/mg] radiation damage ([A-C] lower panels). (ZM = zircon morphology). (Individual boxes represent one-second increments within a single analysis, 2-sigma). Pit ablation depth estimated based on previous laboratory calibration measurements using a Bruker Optical Profilometer. (B) Wetherill Concordia plot (1956) for each individual, complete, analyses (30/40 s). (Tera Wasserburg diagrams are visualized in Fig. S3).

integration of the U and Th concentrations (and respective α-decay doses) within the depth profiles show that the variability of the age domains are mostly mirrored by trace element concentrations (Figs. 3A, 4A, 5A–C). In addition, U and Th concentrations are notably higher in zircon crystals displaying relatively higher levels of alteration, becoming apparent in: (1) less well developed age plateaus (increased scatter and MSWD respectively); and/or (2) a zircon morphology described as fractured (ZM = 2) (Fig. 6).

5. Discussion

We illustrate that the U-Pb depth profiling LA-ICP-MS analysis presented here has the potential to reveal spatially-resolved information about the complex history of individual zircon crystals affected by a hypervelocity impact event. Three key questions arise, which are discussed in more detail below: Section 5.1.) Can LA-ICP-MS depth profiling deconvolve complex age domains in zircon crystals, including Pb loss effects? Section 5.2.) What is the effect of high U (and Th) concentrations on age preservation or resetting in response to an impact? And Section 5.3.) what effect does radiation damage, based on calculated α-decay radiation damage accumulation, have on the crystal annealing temperatures in the setting of an impact crater?

5.1. Can LA-ICP-MS depth profiling deconvolve complex age domains in zircon crystals, including Pb loss effects?

The data reduction scheme adopted here allows for the interpretation of U-Pb data in discrete one-second steps, and for assessment of whether spatial variations in age correlate with trace element heterogeneities in individual zircon crystals. Our results suggest that weighted mean ages based on traditional LA-ICP-MS data reduction schemes likely would mask pertinent age information by integrating and averaging domains with different ages and limiting the ability to identify spatial inhomogeneities preserved within altered zircons. For example, the decay of zoned trace elements U and Th causes spatially heterogeneous levels of radiation damage and metamictization within zircon crystals, since those trace elements are not homogeneously distributed (e.g., Nasdala et al., 1996; Woodhead et al., 1991). Similar to previous

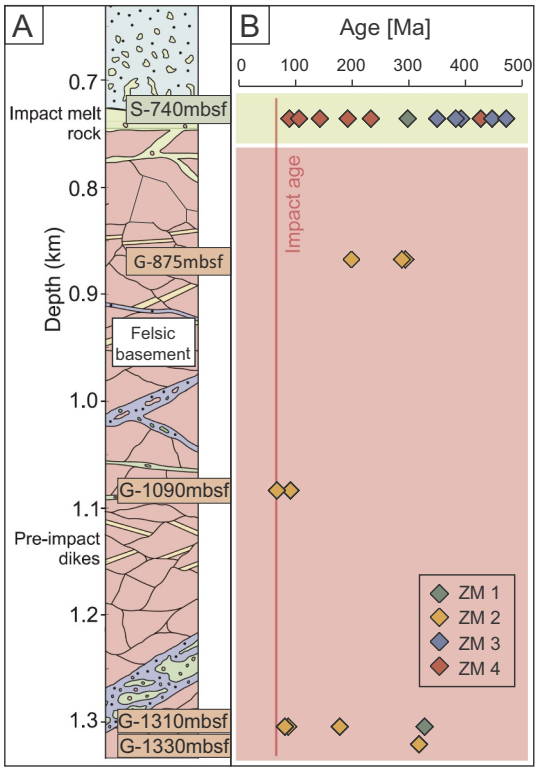

Fig. 6. Results summary. (A) Stratigraphic section of the drill core recovered by IODP Exp. 364 (modified from Morgan et al., 2016) with marked sample locations. (B) $^{206}Pb/^{238}U$ weighted mean ages of zircon material analyzed in this study, color-coded based on the described zircon morphology (ZM 1 = virtually undeformed, ZM 2 = irregular fractured, ZM 3 = planar fractured, ZM 4 = granular textured).

studies (e.g., Schwarz et al., 2016; Schmieder et al., 2019), our results suggest that metamictization appears to significantly influence impact-induced Pb loss.

While any single 'one-second age domain' can be an artifact of age mixing, the spatial topology of the weighted mean ages, obtained from continuous age domains that form age plateaus, provide a more robust and meaningful method to evaluate and calculate reliable mean ages (Spencer et al., 2016). Moreover, one-second increment pacing, and the subsequent data visualization as age spectra plots, rigorously identifies any inhomogeneities within individual zircons, which becomes apparent both in zircon crystals that are analyzed twice, and during the selection of plateaus to calculate weighted mean ages (Figs. 3A, 4A, 5A–C).

Setting ideal laser parameters during the experiment is essential to obtain robust age data that allow for a reliable age interpretation based on one-second data increments. The primary resolution limitation for small ablation spots paired with low ablation frequency (e.g., 10 Hz) is the washout time, i.e., the time it takes for the signal to return to pre-ablation levels at the end of a laser pulse (e.g., Horstwood et al., 2003). This is of particular importance for the here applied continuous, non-pulses depth-profiling approach as it controls the time and depth resolution during progressive ablation and hence the ages that can be resolved without 'smearing'. For the instrumental setup and conditions used, washout times were determined to be < 0.5 s post-ablation (return to < 5× the background). With a determined ablation rate of ~0.5 μm/s, we feel confident that ablation intervals of down to 0.3 μm could be readily resolved and that one-second data increments are conservative, allowing for > 2× the nominal washout time.

It is evident from our data that younger depth-profiled age domains are characterized by a higher U concentration [ppm] and consequently greater levels of radiation damage (i.e., metamictization), appearantly leading to the incorporation of common Pb into the damaged zones. Alternatively, such an increase in U, Th, and common Pb concentrations could also point towards metamorphic - and in case of an impact structure hydrothermal - fluid flow leading to mineral growth and recrystallization along zircon surfaces and fractures. In such a scenario, an increase in common Pb would indicate "volatile-rich" fluids (Breeding et al., 2004; Kelly et al., 2014). Independent of a possible cause, the coupled higher U and common Pb concentrations are also reflected by an increased degree in discordance - becoming apparent in divergent $^{206}Pb/^{238}U$ and $^{207}Pb/^{235}U$ ages that plot below the Concordia curve (Wetherill, 1956) - requiring a larger common Pb correction (e.g., Nasdala et al., 1998). Within the age data presented in this study, concordant ages are largely associated with zircon domains that show less evidence for metamictization and alteration, whereas age domains with higher discordance can be directly linked to zones with high U concentrations that experienced Pb loss related to thermal events, in particular regional tectonism and the K-Pg impact event. Consequently, while low-damage zircon data are mostly concordant and preserve the pre-impact U-Pb signature, metamict and/or fluid altered zircon crystals or domains affected by post-300 Ma events are generally more discordant and require a more significant common Pb correction. This phenomenon is accentuated by the inherent imprecision of the $^{207}Pb/^{235}U$ measruments that therefore are more strongly affected by common Pb (e.g., Bowring and Schmitz, 2003; Spencer et al., 2016). Interestingly, all but one depth-profile analysis in this study showed an overall decrease in U and Th concentrations with increasing ablation time/depth, after standard-based elemental downhole fraction correction using GJ-1 zircon analyzed with identical instrumental settings (Figs. 3A, 4A, 5A/C). While measured Pb/U exhibits a time-dependent evolution, depending on a number of factors, including ablation pit size, ablation rate, sample gas flows, and chemical characteristics of different elements during progressive ablation (e.g., Paton et al., 2010), we are confident that the downhole-corrected depth profiles accurately display a decrease in U and Th concentrations. This behavior is not a systemic artifact of depth-profiling, but clearly related to the particular zircon petrogenesis, likely caused by progressive magma fractionation. However, U-Pb SIMS depth profiling has also demonstrated the U and Th increase at grain edges on the micron-scale, interpreted as secondary zircon precipitation due to metamorphic-induced fluid flow (Breeding et al., 2004; Kelly et al., 2014; Skipton et al., 2016). Progressively decreasing U and Th concentrations have also been reported in zircon from CA-TIMS U-Pb step dissolution experiments (Mattinson, 2005), with U and Th concentrations being higher in initial leachates of stepwise dissolutions. This effect, however, appears to be linked to preferential dissolution of high-U metamict zones, as demonstrated by imaging of partially-digested grains. Similarly, though, these initial step ages are also associated with a higher discordance and incorporation of common Pb, whereas the subsequent dissolution steps display progressively lower U and Th concentrations and ages with decreased discordance (e.g., Mundil et al., 2004).

The zircon crystals in this study are relatively small (≤ 35 μm in length), especially those from the granitoid rocks of the lower half of the core (1090–1330 mbsf), meaning only one laser spot, with a diameter of 25 μm, could be placed on the prism surface. We consider 25 μm to be the smallest viable ablation spot size to acquire a large enough sample volume to obtain sufficient analytical precision to interpret meaningful age data. Hence, during the analyses a relativley large portion of the crystal volume was consumed by the ablation and the petrographic context of the mineral was, as a result, disturbed or lost. Nonetheless, our analytical approach enables us to extract fundamental information from the zircon crystals, allowing us to quantify rim and center ages in relationship to U and Th concentrations. However, for future work, it would desirable to pair LA-ICP-MS depth profiling with crystal petrography, such as high-resolution EBSD mapping, and in-situ thin section analysis (e.g., Timms et al., 2012, 2017; Cavosie

et al., 2016, 2018; Erickson et al., 2017; Kenny et al., 2017). (See also Section 5.2.).

U-Pb LA-ICP-MS is considered an efficient method to obtain spatially varying isotope data within zircon (e.g., Kelly et al., 2014; Marsh and Stockli, 2015; this study). However, the method faces certain obstacles in comparison to spot size techniques that allow for a smaller amount of sample material to be analyzed, such as SIMS U-Pb depth profiling or atom probe tomography (Grove and Harrison, 1999; Breeding et al., 2004; Abbott et al., 2012; Kelly et al., 2014; Skipton et al., 2016; Montalvo et al., 2019). Whereas Kelly et al. (2014) showed that LA-ICP-MS depth profiling is able to re-produce results previously obtained by SIMS U-Pb depth profiling, they also demonstrated that especially very thin (nm thick) crystal rims cannot be as well resolved via the LA-ICP-MS depth profiling method. Secondary mineral growth or recrystallization caused by fluid flow, be it in a tectono-thermal or in an impact-induced hydrothermal setting, is commonly nm think and located along the mineral surface or fractures (e.g., Grove and Harrison, 1999; Breeding et al., 2004; Abbott et al., 2012; Kelly et al., 2014). While SIMS U-Pb depth profiling has the advantage by being able to readily resolve depth profiles of 50–100 nm (with a depth profile depth commonly being ~5 μm) and provide U-Pb age constrains or trace element concentrations for very thin (~0.4–4 μm; Skipton et al., 2016) mineral rims (Breeding et al., 2004; Kelly et al., 2014; Skipton et al., 2016), it is practically limited in terms of depth penetration and resolving grain interiors. Atom probe tomography is able to semi-quantitatively identify local enrichment in trace element concentration on the nanoscale for example within reidite lamellae in shocked zircon, again LA-ICP-MS depth profiling is not able to resolve information on this scale. However, SIMS and atom probe tomography face challenges when it comes to analyzing interior age domains of unpolished mineral specimens. LA-ICP-MS analysis has the advantage of easily and rapidly generating depth-profile data from rim to center of entire grains, allowing for spatially resolution of age domains within the crystal interior without the need of polishing the sample. Whereas SIMS depth profiled are commonly < 5 μm deep, LA-ICP-MS depth profiles, depending on spot size, are viable to > 40 μm depth. While our study corroborates previous findings from SIMS depth-profiling studies showing an increased age variability within the outer rim (e.g., Grove and Harrison, 1999), our data demonstrate the importance of crystal interiors for capturing fundamental age information, such as younger interior age domains reflecting partial age resetting or potentially full age resetting to the proposed impact age (Figs. 3Ab, 4Aa).

In conclusion, the most robust approach to disentangle spatial age distribution is a multi-analyses application consisting of LA-ICP-MS and SIMS depth profiling as well as petrographic analyses, such as by EBSD mapping, in order to unravel geological events preserved within complexly altered zircon populations at a high enough resolution from nm thick rims to the crystal interior. However, LA-ICP-MS depth profiling, and the subsequent data reduction and visualization in one-second increments, is a powerful tool for obtaining high spatial age resolution within zircon crystals, while simultaneously quantifying trace element concentrations. U-Pb depth profiling allows for a rigorous selection of age plateaus, which is especially useful for interpreting highly-altered zircon material, while also representing a useful pre-screening tool for subsequent ID-TIMS (step dissolution) dating or SIMS analyses and, therefore, represents a highly complementary technique to other U-Pb approaches.

5.2. What is the effect of high U and Th zones on age preservation and impact resetting?

In contrast to the crater center with initial shock pressure > 100 GPa, (French, 1998) and initial temperatures ≥1700 °C (Abramov and Kring, 2007), the granitoid peak-ring rocks and lithic breccias experienced lower shock pressure of ~12–17 GPa and only modest heating, making the zircon U-Pb clock less susceptible to resetting due to the impact event and the signatures more subtle (Rae et al., 2017). Only minor volumes of the peak-ring rocks were in direct contact with hot impact melt (and breccias) (e.g., Morgan et al., 2016; Gulick et al., 2017a). However, the Chicxulub peak ring experienced impact-induced hydrothermal overprinting in a hot fluid system that has temperatures of up to 400 °C for a duration of ~1.5–2.3 Myr (Abramov and Kring, 2007). Therefore, it is not misguided to expect at least partial age resetting within the zircon crystals of the peak ring rocks.

A large body of work has focused on the correlation of impact-induced microstructures in zircon and their effect on Pb diffusion, resetting, and corresponding age signals (e.g., Timms et al., 2012, 2017; Schmieder et al., 2015; Kovaleva et al., 2015; Cavosie et al., 2015; Kenny et al., 2019). Previous studies of shock metamorphic microstructures reported a link between age resetting and the degree of shock metamorphism, with highly shocked zircon crystals being age reset by shock pressure (≥59 GPa; Deutsch and Schärer, 1990), in combination with resetting due to post-impact heating and/or by being embedded or grown (neoblast) within the melt sheet (e.g., Krogh et al., 1993a, 1993b; Kamo et al., 1996; Kalleson et al., 2009; Schmieder et al., 2015; Schmieder et al., 2018; Kenny et al., 2019).

Our study, however, also suggests a link between younger age domains and higher U and Th concentrations that occur in fractured zircon crystals (Table 1). However, fracturing cannot be considered a diagnostic feature for shock metamorphism, since it can also be caused by other processes, including radiation damage (Timms et al., 2012). Since trace elements, including U and Th, are heterogeneously distributed within zircon crystals, so is the resulting radiation damage caused by U and Th decay (i.e., metamictization) (e.g., Nasdala et al., 1996). Radiation-induced alpha decay damage, mainly related to recoil, causes the formation of amorphous and quasi-amorphous regions within the mineral lattice, which in turn cause a decrease in density and elasticity, while increasing brittle behavior (Holland and Gottfried, 1955; Chakoumakos et al., 1987). In addition, Holland and Gottfried (1955) argue that such radiation-induced recrystallization leads to a volume expansion and hydration of U-rich zones in zircon, which in turn causes fracturing within non-metamict, more resistant, low-U zones of the zircon crystal. Radiation damage facilitates Pb diffusion within the damaged mineral zones, which becomes apparent as an increase in discordance (e.g., Silver and Deutsch, 1963; McLaren et al., 1994). Therefore, we suggest that the fracturing observed in some zircon crystals could be related to the impact or be the result of radiation damage within the crystal. In either case, the radiation damage facilitated the diffusive loss of radiogenic Pb by lowering the diffusion temperature from ~900 °C in non-damaged, pristine zircon to temperatures possibly lower than 200 °C (e.g., Cherniak et al., 1991; Meldrum et al., 1998; Geisler et al., 2001; Pidgeon, 2014) (see also Section 5.3). We observe that the impact likely caused partial age resetting (88 ± 3.1 Ma, [G-1090mbsf-1]; 86 ± 5.0 Ma, 80 ± 3.0 Ma, [G-1310mbsf-2]), and possibly full age resetting (66 ± 6.2 Ma, [G-1090mbsf-1]) within shocked zircon crystals previously affected by radiation damage (Figs. 4A) (compare Schwarz et al., 2016; Schmieder et al., 2019). However, fracturing due to the passage of the shock wave or even due to the sample processing cannot be ruled out.

The results of the zircon crystals extracted from the impact melt rock demonstrate that the U-Pb clock is partially reset (M-740mbsf-2A, B/−3A, B). The partial age resetting becomes apparent either by relatively young ages (youngest age: 88 ± 5.9 Ma, M-740mbsf-2B) or possibly by age mixing within the crystal rim (M-740mbsf-1). Whether or not some of the weighted mean ages are relics of regional metamorphism, for example Silurian or Triassic and Jurassic intrusions, is difficult to evaluate. However, previous U-Pb studies on Chicxulub demonstrated that the impact event produced a wide variety of ages, ranging from crystalline basement (~550 Ma) down to post-impact ages (~57 Ma, lower concordia intercept age) (e.g., Krogh et al., 1993a, 1993b; Kamo et al., 2011; Schmieder et al., 2018).

Previous studies showed that zircon crystals displaying granular textures are often linked to relatively young ages, including the proposed impact age, suggesting that the formation of granular textures is driven by the level of shock and associated high post-shock temperatures, which is possibly enhanced in zircon zones with a high U concentration (e.g., Wittmann et al., 2006; Cavosie et al., 2015; Schmieder et al., 2015; Cavosie et al., 2016; Timms et al., 2017; Kenny et al., 2019). Moreover, the breakdown of zircon and the subsequent polycrystalline recrystallization displayed as a granular texture promotes Pb loss (Krogh et al., 1993a, 1993b; Kamo et al., 1996; Tohver et al., 2012, Kalleson et al., 2009; Schmieder et al., 2015; Cavosie et al., 2015, 2018). According to e.g., Cavosie et al. (2015), the formation of granular textures is not restricted to the shock metamorphic realm and can also occur due to tectonic deformation. Independent of their origin, granular crystals display the same exterior features, while the most significant difference is that granular textures not produced by impacts tend to preserve younger rims around an inherited zircon core, whereas granular zircon that formed due to shock metamorphism consists partily or entirely of neoblasts (Cavosie et al., 2015). In order to unequivocally distinguish between the two types a detailed mineralogical analysis of the crystals in question is indispensable (e.g., Cavosie et al., 2015; Kenny et al., 2019). Nevertheless, the crystals in this study showing granular textures, display both younger rim and older core ages along with relatively moderate U concentrations (~300 ppm, [Table 1]) (Figs. 3Ab, 5A). This suggests, since granules facilitate Pb loss, that their U-Pb clock was only partially reset due to the impact event with a youngest weighted mean age of 88 ± 5.9 Ma, [M-740mbsf-2B]. This result is unsurprising since previously reported ages from granular zircon crystals from Chicxulub were also associated with an age relativeley close to the proposed impact age (Krogh et al., 1993b).

To draw further conclusions about the formation of granular zircon, high resolution EBSD mapping in combination with SEM and CL-imaging has been shown to be critical (e.g., Cavosie et al., 2016, 2018; Erickson et al., 2017; Timms et al., 2017; Kenny et al., 2017, 2019). This can yield fundamental insights into pressure and temperature conditions that a zircon crystal experienced during the time of impact. For example, the preservation of so called “FRIGN” zircon (“former reidite in granular neoblastic”) indicates high temperatures (≥1200 °C) and high pressure conditions (≥30 GPa) (Cavosie et al., 2018), whereas the formation of lamellar redeite point towards high pressures (≥30 GPa) but lower temperatures (< 1200 °C) (Erickson et al., 2017; Timms et al., 2017).

In contrast, in this study, a crystal displaying possible planar fracturing appears to record no age resetting due to the impact event, with ages ranging from 472 ± 4.4 Ma (S-740mbsf-3B) to 350 ± 11 Ma (S-740mbsf-3A) (Fig. 5B). Those ages are instead linked to either the basement age (550–570 Ma, Krogh et al., 1993a, 1993b), or Silurian-(~418 Ma, Bateson, 1972; Steiner and Walker, 1996) and Carboniferous intrusion ages (~300–340 Ma, Xiao et al., 2017). Since Pb loss in zircon displaying planar microstructures can be irregular (Cavosie et al., 2015), it is possible that we either did not ablate an area within the crystal that had been reset or that the crystal has not been reset by the impact event. The latter is more likely amid the high degree of concordance associated with both analyses (Fig. 5D).

Hence, in conclusion, factors such as partial age resetting, discordance, and a non-systematic Pb loss behavior make the determination of impact ages challenging. This study demonstrates that U-Pb depth profiling can reveal heterogeneously distibuted age domains within shocked zircon crystals. However, high U (and Th) zones in fractured zircon are more prone to resetting and preservation of younger ages, and possibly even the impact age. Crystals displaying granular textures appear to facilitate Pb diffusion in response to the impact event, but in our study, their formation cannot be solely linked to high U (or Th) concentrations as previously suggested by other studies (e.g., Kalleson et al., 2009; Schmieder et al., 2015). Moreover, our data demonstrate that younger Pb-loss ages are not restricted to the crystal rims, but are rather spatially correlated with zones of high U (or Th) concentration, independent of their location within the crystal (Figs. 3Ac, 4Aa/c, 5B). The results demonstrate that obtaining an reliable impact age from a variable shocked zircon population is challenging as the population can be dominated by bulk U-Pb ages reflecting the age of the target rock or other pre-impact thermal events (see also Petrus et al., 2016). However, radioisotopic analyses of the granitoid basement of the IODP Exp. 364 cores has shown that the drilled basement rocks of the peak ring are Carboniferous in age (Xiao et al., 2017; this study) rather than Late Paleozoic rocks associated with the Maya block ages (Kettrup and Deutsch, 2003). Therefore, a previously unknown target rock component was identified.

5.3. What is the effect of radiation damage on the Pb loss temperatures in an impact crater setting?

Table 1 (and Table S1) summarizes the α-decay doses calculated for this study. Based on those α-decay doses, the peak ring zircon crystals can be classified as Stage 1, where radiation damage occurs primarily as “isolated point defects” (α-decay dose ≤ 3×10^{15} α/mg) or as beginning Stage 2, where the amount of amorphous material is increased while the remaining crystalline material is distorted (α-decay dose 2.2–5 × 10^{15} α/mg) (Holland and Gottfried, 1955; Murakami et al., 1991; Nasdala et al., 2004; Pidgeon, 2014, and references within [also for definition of radiation damage stages]). Beginning Stage 2 radiation damage is found in four analyses (of three crystals) that are primarily associated with the youngest ages (G-1090mbsf-1; G-1310mbsf-1) (Table 1) (Figs. 4A). Therefore, it can be hypothesized that the majority of the zircon crystals analyzed for this study are crystalline (pristine) with isolated amorphous zones, while the two crystals yielding the youngest ages may have already developed an amorphous network within the mineral lattice (Murakami et al., 1991).

Crystal annealing temperatures are lowered within amorphous zircon zones caused by radiation damage (metamictization) (e.g., Holland and Gottfried, 1955; Weber, 1990; Murakami et al., 1991; Salje et al., 1999; Davis and Krogh, 2001; Geisler et al., 2001, Nasdala et al., 2004; Rios et al., 2000; Pidgeon, 2014). In crystalline zircon, Pb diffusion is considered a slow process that requires high temperatures of, at least, ~900 °C for ~1 Myr to produce significant Pb loss (Cherniak and Watson, 2001). However, diffusion in metamict zircon occurs more rapidly and at lower temperatures, which have been proposed to range from 150 °C to 350 °C (Cherniak et al., 1991; Meldrum et al., 1998; Davis and Krogh, 2001; Geisler et al., 2001; Moser et al., 2011; Pidgeon, 2014 [and references therein]). A specific temperature at which crystals anneal due to radiation damaged zones cannot be assumed, however, a ‘partial annealing zone’ consisting of a range of temperatures has to be expected (Bernet and Garver, 2005; Pidgeon, 2014). Since the peak ring rocks were buried at a depth of 8–10 km pre-impact they must have experienced temperatures of, at least, 200–250 °C, assuming a thermal gradient of only 20–25 °C/km (Morgan et al., 2016). Since the zircon U-Pb system was not reset under those pre-impact crustal conditions, it can be assumed that either the annealing temperature of zircon preserving Stage 1 radiation damage is, at least, 250–300 °C, as proposed by Davis and Krogh (2001) or that the heat pulse due to the impact event of at least ~1200 °C within the first seconds after the impact (Onorato et al., 1978; Abramov and Kring, 2007) facilitated the (partial) resetting of the zircon U-Pb clock. In addition, the impact-induced hydrothermal system might also have contributed to (partial) resetting. For Chicxulub, numerical modeling has pointed towards a duration of ~1.5–2.3 Myr (Abramov and Kring, 2007) for the hydrothermal systems with temperatures ranging between 200-400 °C, as bracketed by high- and low-temperature alternation minerals preserved in IODP Exp. 364 (Kring et al., 2017a, 2017b; Schmieder et al., 2018). These conditions were well within the range of promoting (partial) resetting in zircon crystals that experienced radiation damage. In addition, hydrothermal fluid flow might also have led to zircon overgrowth or

recrystallization enriched in U, Th, and common Pb at the surface or in fractures (Breeding et al., 2004; Kelly et al., 2014).

6. Conclusion

The zircon U-Pb age domains from the granitoid rocks and an impact melt rock sample from the peak ring of the Chicxulub impact structure reveal a complex alteration history and a wide range of inherited basement ages, including those of previously unknown Carboniferous target rocks, as well as pre-, *syn*-, and post-impact age domains and weighted mean ages. Our results suggest that shock metamorphism and concomitant impact induced heating preferentially affects radiation damaged (metamict) zones within the zircon crystals. Thus, impact-induced age resetting in zircon might be more likely observed in regions affected by intra-grain U-Pb kinetics. However, further detailed petrographic studies are necessary.

It can be concluded that impact-induced shock metamorphism (shock pressure and heating) resulted in annealing of metamict zircon zones that were more prone to resetting during a thermal event and not necessarily within crystals that display a specific morphology. Shock induced crystal annealing facilitates Pb diffusion to the point that some age domains yielded the Chicxulub impact age of 66 ± 6.2 Ma (e.g., G-1090mbsf-1). These results suggest that metamict domains in zircon can record episodes of impact metamorphism and, in consequence, affect the age preservation of impact events.

The calculated α-decay doses show that most zircon crystals are expected to have experienced Stage 1 and early Stage 2 radiation damage accumulation, which would cause a reduced Pb diffusion temperature of and order of 250–300 °C. This and/or the short-lived high-temperature heat pulse due to the impact event or hot-fluid flow in the impact-induced hydrothermal system may have facilitated resetting of the U-Pb clock in zircon crystals or zircon domains that experienced radiation damage or display granular textures.

Acknowledgements

This research used samples and data provided by IODP. Samples can be requested at http://web.iodp.tamu.edu/sdrm. Expedition 364 was jointly funded by the European Consortium for Ocean Research Drilling (ECORD) and the International Continental Scientific Drilling Program, with contributions and logistical support from the Yucatán State Government and Universidad Nacional Autónoma de México (UNAM). This research was supported by the U.S. Science Support Program and NSF grant OCE-1737351. We would also like to thank Lisa Stockli and James Maner for their help and support while conducting our analyses at the UT Austin laboratories. We also thank Kenny Gavin and one anonymous reviewer for their valuable comments on the manuscript and in particular the editor, Balz Kamber, for his suggestions and support to improve this work. This is UTIG Contribution no. 3512 and LPI Contribution no. 2191.

Appendix A. Supplementary data

Supplementary data to this article can be found online at https://doi.org/10.1016/j.chemgeo.2019.07.029.

References

Abbott, S.S., Harrison, T.M., Schmitt, A.K., Mojzsis, S.J., 2012. A search for thermal excursions from ancient extraterrestrial impacts using Hadean zircon Ti-U-Th-Pb depth profiles. Proc. Natl. Acad. Sci. 109, 13486–13492.
Abramov, O., Kring, D.A., 2007. Numerical modeling of impact-induced hydrothermal activity at the Chicxulub crater. Meteorit. Planet. Sci. 42, 93–112.
Alvarez, L.W., Alvarez, W., Asaro, F., Michel, H.V., 1980. Extraterrestrial Cause for the Cretaceous-Tertiary Extinction. Science 208, 1095–1108.
Andersen, T., 2002. Correction of common lead in U-Pb analyses that do not report ^{204}Pb. Chem. Geol. 192, 59–79.
Bateson, J.H., 1972. New interpretation of geology of Maya Mountains, British Honduras. AAPG Bull. 56, 956–963.
Bernet, M., Garver, J.I., 2005. Fission-track analysis of detrital zircon. Rev. Mineral. Geochem. 58, 205–237.
Bland, P.A., 2005. The impact rate on Earth. Philosophical Transactions of the Royal Society of London A: Mathematical, Physical and Engineering Sciences 363, 2793–2810.
Bowring, S.A., Schmitz, M.D., 2003. High-precision U-Pb zircon geochronology and the stratigraphic record. Rev. Mineral. Geochem. 53, 305–326.
Breeding, C.M., Ague, J.J., Grove, M., Rupke, A.L., 2004. Isotopic and chemical alteration of zircon by metamorphic fluids: U-Pb age depth-profiling of zircon crystals from Barrow's garnet zone, northeast Scotland. Am. Mineral. 89, 1067–1077.
Cavosie, A.J., Erickson, T.M., Timms, N.E., Reddy, S.M., Talavera, C., Montalvo, S.D., Pincus, M.R., Gibbon, R.J., Moser, D., 2015. A terrestrial perspective on using ex situ shocked zircons to date lunar impacts. Geology. 43, 999–1002.
Cavosie, A.J., Timms, N.E., Erickson, T.M., Hagerty, J.J., Hörz, F., 2016. Transformations to granular zircon revealed: Twinning, reidite, and ZrO_2 in shocked zircon from Meteor Crater (Arizona, USA). Geology 44, 703–706.
Cavosie, A.J., Timms, N.E., Ferrière, L., Rochette, P., 2018. FRIGN zircon - the only terrestrial mineral diagnostic of high-pressure and high-temperature shock deformation. Geology 46, 891–894.
Chakoumakos, B.C., Murakami, T., Lumpkin, G.R., Ewing, R.C., 1987. Alpha-decay - Induced fracturing in zircon: the transition from the crystalline to the metamict state. Science 236, 1556–1559.
Cherniak, D.J., Watson, E.B., 2001. Pb diffusion in zircon. Chem. Geol. 172 (1-2), 5–24.
Cherniak, D.J., Lanford, W.A., Ryerson, F.J., 1991. Lead diffusion in apatite and zircon using ion implantation and Rutherford backscattering techniques. Geochim. Cosmochim. Acta 55, 1663–1673.
Compston, W., Williams, I.S., Jenkins, R.J.F., Gostin, V.A., Haines, P.W., 1987. Zircon age evidence for the Late Precambrian Acraman ejecta blanket. Aust. J. Earth Sci. 34 (4), 435–445.
Davis, D.W., Krogh, T.E., 2001. Preferential dissolution of ^{234}U and radiogenic Pb from α-recoil-damaged lattice sites in zircon: implications for thermal histories and Pb isotopic fractionation in the near surface environment. Chem. Geol. 172, 41–58.
Deutsch, A., Schärer, U., 1990. Isotope systematics and shock-wave metamorphism: I. U-Pb in zircon, titanite and monazite, shocked experimentally up to 59 GPa. Geochim. Cosmochim. Acta 54, 3427–3434.
Deutsch, A., Schärer, U., 1994. Dating terrestrial impact events. Meteorit. Planet. Sci. 29, 301–322.
Erickson, T.M., Pearce, M.A., Reddy, S.M., Timms, N.E., Cavosie, A.J., Bourdet, J., Rickard, W.D.A., Nemchin, A.A., 2017. Microstructural constraints on the mechanisms of the transformation to reidite in naturally shocked zircon. Contrib. Mineral. Petrol. 172, 1–26.
Farmer, J.D., 2000. Hydrothermal systems: doorways to early biosphere evolution. GSA Today 10, 1–9.
French, B.M., 1998. Traces of Catastrophe: A Handbook of Shock-Metamorphic Effects in Terrestrial Meteorite Impact Structures. Technical Report, LPI/NASA (132 pp).
Geisler, T., Pidgeon, R.T., van Bronswijk, W., Pleysier, R., 2001. Kinetics of thermal recovery and recrystallization of partially metamict zircon: a Raman spectroscopic study. Eur. J. Mineral. 13, 1163–1176.
Gradstein, F.M., 2012. Introduction. In the Geologic Time Scale. Elsevier, pp. 1–29.
Grove, M., Harrison, M.T., 1999. Monazite Th-Pb age depth profiling. Geology 27, 487–490.
Gulick, S.P.S., Christeson, G.L., Barton, P.J., Grieve, R.A.F., Morgan, J.V., Urrutia-Fucugauchi, J., 2013. Geophysical characterization of the Chicxulub impact crater. Rev. Geophys. 51, 31–52.
Gulick, S., Morgan, J., Mellett, C.L., Green, S.L., Bralower, T., Chenot, E., Christeson, G., Claeys, P., Cockell, C., Coolen, M., Ferrière, L., Gebhardt, C., Goto, K., Jones, H., Kring, D., Lofi, J., Lowery, C., Ocampo-Torres, R., Perez-Cruz, L., Pickersgill, A.E., Poelchau, M., Rae, A., Rasmussen, C., Rebolledo-Vieyra, M., Riller, U., Sato, H., Smit, J., Tikoo, S., Tomioka, N., Urrutia-Fucugauchi, J., Whalen, M., Wittmann, A., Yamaguchi, K., Xiao, L., Zylberman, W., 2017a. Site M0077: Lower Peak Ring. vol. 364. International Ocean Discovery Program, College Station, TX, pp. 2377–3189.
Gulick, S., Morgan, J., Mellett, C.L., the Expedition 364 Scientists, 2017b. Expedition 364 Preliminary Report: Chicxulub: Drilling the K-Pg Impact Crater. https://doi.org/10.14379/iodp.pr.364.2017.
Hildebrand, A.R., Penfield, G.T., Kring, D.A., Pilkington, M., Camargo Z, A., Jacobsen, S. B. and Boynton, W.V., 1991. Chicxulub crater: a possible Cretaceous/Tertiary boundary impact crater on the Yucatan Peninsula, Mexico. Geology. 19, 867–871.
Holland, H.D., Gottfried, D., 1955. The effects of nuclear radiation on the structure of zircon. Acta Cryst 8, 291–300.
Horstwood, M.S., Foster, G.L., Parrish, R.R., Noble, S.R., Nowell, G.M., 2003. Common-Pb corrected in situ U-Pb accessory mineral geochronology by LA-MC-ICP-MS. J. Anal. At. Spectrom. 18, 837–846.
Horstwood, M.S., Košler, J., Gehrels, G., Jackson, S.E., McLean, N.M., Paton, C., Pearson, N.J., Sircombe, K., Sylvester, P., Vermeesch, P., Bowring, J.F., 2016. Community-derived standards for LA-ICP-MS U-(Th-)Pb geochronology - uncertainty propagation, age interpretation and data reporting. Geostand. Geoanal. Res. 40, 311–332.
Jackson, S.E., Pearson, N.J., Griffin, W.L., Belousova, E.A., 2004. The application of laser ablation-inductively coupled plasma-mass spectrometry to in situ U–Pb zircon geochronology. Chem. Geol. 211, 47–69.
Jourdan, F., 2012. The ^{40}Ar/^{39}Ar dating technique applied to planetary sciences and terrestrial impacts. Aust. J. Earth Sci. 59 (2), 199–224.
Jourdan, F., Renne, P.R., Reimold, W.U., 2009. An appraisal of the ages of terrestrial impact structures. Earth Planet. Sci. Lett. 286 (1–2), 1–13.
Jourdan, F., Reimold, W.U., Deutsch, A., 2012. Dating terrestrial impact structures. Elements 8 (1), 49–53.

Kalleson, E., Corfu, F., Dypvik, H., 2009. U-Pb systematics of zircon and titanite from the Gardnos impact structure, Norway: evidence for impact at 546 Ma? Geochim. Cosmochim. Acta 73, 3077–3092.
Kamo, S.L., Krogh, T.E., 1995. Chicxulub crater source for shocked zircon crystals from the Cretaceous-Tertiary boundary layer, Saskatchewan: evidence from new U-Pb data. Geology 23, 281–284.
Kamo, S.L., Reimold, W.U., Krogh, T.E., Colliston, W.P., 1996. A 2.023 Ga age for the Vredefort impact event and a first report of shock metamorphosed zircons in pseudotachylitic breccias and granophyre. Earth Planet. Sci. Lett. 144, 369–387.
Kamo, S.L., Lana, C., Morgan, J.V., 2011. U–Pb ages of shocked zircon grains link distal K–Pg boundary sites in Spain and Italy with the Chicxulub impact. Earth Planet. Sci. Lett. 310, 401–408.
Kelly, C.J., McFarlane, C.R., Schneider, D.A., Jackson, S.E., 2014. Dating micrometre-thin rims using a LA-ICP-MS depth profiling technique on zircon from an Archaean metasediment: comparison with the SIMS depth profiling method. Geostandards and GeoanalyticalResearch 38, 389–407.
Kenny, G.G., Morales, L.F., Whitehouse, M.J., Petrus, J.A., Kamber, B.S., 2017. The formation of large neoblasts in shocked zircon and their utility in dating impacts. Geology 45, 1003–1006.
Kenny, G.G., Schmieder, M., Whitehouse, M.J., Nemchin, A.A., Morales, L.F., Buchner, E., Bellucci, J.J., Snape, J.F., 2019. A new U–Pb age for shock-recrystallised zircon from the Lappajärvi impact crater, Finland, and implications for the accurate dating of impact events. Geochim. Cosmochim. Acta 245, 479–494.
Keppie, J.D., Dostal, J., Norman, M., Urrutia-Fucugauchi, J., Grajales-Nishimura, M., 2011. Study of melt and a clast of 546 Ma magmatic arc rocks in the 65 Ma Chicxulub bolide breccia, northern Maya block, Mexico: western limit of Ediacaran arc peripheral to northern Gondwana. Int. Geol. Rev. 53, 1180–1193.
Kettrup, B., Deutsch, A., 2003. Geochemical variability of the Yucatán basement: Constraints from crystalline clasts in Chicxulub impactites. Meteorit. Planet. Sci. 38, 1079–1092.
Kovaleva, E., Klötzli, U., Habler, G., Wheeler, J., 2015. Planar microstructures in zircon from paleo-seismic zones. Am. Mineral. 100, 1834–1847.
Kring, D.A., 2007. The Chicxulub impact event and its environmental consequences at the Cretaceous–Tertiary boundary. Palaeogeogr. Palaeoclimatol. Palaeoecol. 255 (1-2), 4–21.
Kring, D.A., Schmieder, M., Shaulis, B.J., Riller, U., Cockell, C., Coolen, M.J.L., the IODP-ICDP Expedition 364 Science Party, 2017a. Probing the impact-generated hydrothermal system in the peak ring of the Chicxulub Crater and its potential as a habitat. In: Lunar and Planetary Science Conference. 48, Abstract No. 1212.
Kring, D.A., Schmieder, M., Riller, U., Simpson, S.L., Osinski, G.R., Cockell, C., Coolen, J.L., the Expedition 364 Science Party, 2017b. Testing a model of impact-generated hydrothermal systems with IODP-ICDP Expedition 364 to the Chicxulub Crater. In: 80th Annual Meeting of the Meteoritical Society, 1987, Abstract No. 6064.
Krogh, T.E., Kamo, S.L., Sharpton, V.L., Marin, L.E., Hildebrands, A.R., 1993a. U-Pb ages of single shocked zircons linking distal K/T ejecta to the Chicxulub crater. Nature 366, 731–734.
Krogh, T.E., Kamo, S.L., Bohor, B.A., 1993b. Fingerprinting the K/T impact site and determining the time of impact by U-Pb dating of single shocked zircons from distal ejecta. Earth Planet. Sci. Lett. 119, 425–429.
Lopez, R., Cameron, K.L., Jones, N.W., 2001. Evidence for Paleoproterozoic, Grenvillian, and Pan-African age Gondwanan crust beneath northeastern Mexico. Precambrian Res. 107, 195–214.
Ludwig, K., 2008. Isoplot/Ex Version 3.7. A Geochronological Toolkit for Microsoft Excel. Berkeley Geochronological Centre, Special Publication.
Marsh, J.H., Stockli, D.F., 2015. Zircon U-Pb and trace element zoning characteristics in an anatectic granulite domain: Insights from LA-ICP-MS depth profiling. Lithos 239, 170–185.
Mattinson, J.M., 2005. Zircon U–Pb chemical abrasion ("CA-TIMS") method: combined annealing and multi-step partial dissolution analysis for improved precision and accuracy of zircon ages. Chem. Geol. 220, 47–66.
McLaren, A.C., Gerald, J.F., Williams, I.S., 1994. The microstructure of zircon and its influence on the age determination from Pb/U isotopic ratios measured by ion microprobe. Geochim. Cosmochim. Acta 58, 993–1005.
Meldrum, A., Boatner, L.A., Weber, W.J., Ewing, R.C., 1998. Radiation damage in zircon and monazite. Geochim. Cosmochim. Acta 62, 2509–2520.
Melosh, H.J., 1989. Impact cratering: a geologic process. Oxf. Monogr. Geol. Geophys. 11, 245.
Mezger, K., Krogstad, E., 1997. Interpretation of discordant U-Pb zircon ages: an evaluation. J. Metamorph. Geol. 15, 127–140.
Montalvo, S.D., Reddy, S.M., Saxey, D.W., Rickard, W.D., Fougerouse, D., Quadir, Z., Johnson, T.E., 2019. Nanoscale constraints on the shock-induced transformation of zircon to reidite. Chem. Geol. 507, 85–95.
Morgan, J., Warner, M., Brittan, J., Buffler, R., Camargo, A., Christeson, G., Dentos, P., Hildebrand, A., Hobbs, R., Macintyre, H., Mackenzie, G., Maguire, P., Marin, L., Nakamura, Y., Pilkington, M., Sharpton, V., Snyder, D., Suarez, G., Trejo, A., 1997. Size and morphology of the Chicxulub impact crater. Nature 390, 472.
Morgan, J.V., Gulick, S.P.S., Bralower, T., Chenot, E., Christeson, G., Claeys, P., Cockell, C., Collins, G.S., Coolen, M., Ferrière, L., Gebhardt, C., Goto, K., Jones, H., Kring, D.A., Le Ber, E., Lofi, J., Xiao, L., Lowery, C., Mellett, C., Ocampo-Torres, R., Osinski, G.R., Perez-Cruz, L., Pickersgill, A., Poelchau, M., Rae, A., Rasmussen, C., Rebolledo-Vieyra, M., Riller, U., Sato, H., Schmitt, D.R., Smit, J., Tikoo, S., Tomioka, N., Urrutia-Fucugauchi, J., Whalen, M., Wittmann, A., Yamaguchi, K.E., Zylberman, W., 2016. The formation of peak rings in large impact craters. Science 354, 878–882.
Moser, D.E., Cupelli, C.L., Barker, I.R., Flowers, R.M., Bowman, J.R., Wooden, J., Hart, J.R., 2011. New zircon shock phenomena and their use for dating and reconstruction of large impact structures revealed by electron nanobeam (EBSD, CL, EDS) and isotopic U-Pb and (U-Th)/He analysis of the Vredefort dome. Can. J. Earth Sci. 48, 117–139.
Mundil, R., Ludwig, K.R., Metcalfe, I., Renne, P.R., 2004. Age and timing of the Permian mass extinctions: U/Pb dating of closed-system zircons. Science 305, 1760–1763.
Murakami, T., Chakoumakos, B.C., Ewing, R.C., Lumpkin, G.R., Weber, W.J., 1991. Alpha decay event damage in zircon. Am. Mineral. 76, 1510–1532.
Nasdala, L., Pidgeon, R.T., Wolf, D., 1996. Heterogeneous metamictization of zircon on a microscale. Geochim. Cosmochim. Acta 60, 1091–1097.
Nasdala, L., Pidgeon, R.T., Wolf, D., Irmer, G., 1998. Metamictization and U-Pb isotopic discordance in single zircons: a combined Raman microprobe and SHRIMP ion probe study. Mineral. Petrol. 62, 1–27.
Nasdala, L., Reiners, P.W., Garver, J.I., Kennedy, A.K., Stern, R.A., Balan, E., Wirth, R., 2004. Incomplete retention of radiation damage in zircon from Sri Lanka. Am. Mineral. 89, 219–231.
Onorato, P.I.K., Uhlmann, D.R., Simonds, C.H., 1978. The thermal history of the Manicouagan impact melt sheet, Quebec. Journal of Geophysical Research: Solid Earth 83, 2789–2798.
Paton, C., Woodhead, J.D., Hellstrom, J.C., Hergt, J.M., Greig, A., Maas, R., 2010. Improved laser ablation U-Pb zircon geochronology through robust downhole fractionation correction. Geochemistry, Geophysics. Geosystems. 11, 1–36.
Paton, C., Hellstrom, J., Paul, B., Woodhead, J., Hergt, J., 2011. Iolite: Freeware for the visualisation and processing of mass spectrometric data. J. Anal. At. Spectrom. 26, 2508–2518.
Petrus, J.A., Kamber, B.S., 2012. VizualAge: a novel approach to laser ablation ICP-MS U-Pb geochronology data reduction. Geostand. Geoanal. Res. 36, 247–270.
Petrus, J.A., Kenny, G.G., Ayer, J.A., Lightfoot, P.C., Kamber, B.S., 2016. Uranium-lead zircon systematics in the Sudbury impact crater-fill: implications for target lithologies and crater evolution. J. Geol. Soc. 173, 59–75.
Pidgeon, R.T., 2014. Zircon radiation damage ages. Chem. Geol. 367, 13–22.
Premo, W.R., Izett, G.A., 1993. U-Pb provenance ages of shocked zircons from the KT boundary, Raton basin, Colorado. In: Lunar and Planetary Science Conference. 24, Abstract No. 1171.
Rae, A.S.P., Morgan, J.V.C., Grieve, R.A., Osinski, G.R. Salge, T., Hall, B., Ferrière, L., Poelchau, M., Gulick, S.P.S., and Exp. 364 Scientists, 2017. Deformation, shock barometry, and porosity within shocked target rocks of the Chicxulub Peak Ring: results from IODP-ICDP Expedition 364. Lunar and Planetary Science Conference. 48, Abstract No. 1934.
Renne, P.R., Deino, A.L., Hilgen, F.J., Kuiper, K.F., Mark, D.F., Mitchell, W.S., Morgan, L.E., Mundil, R., Smit, J., 2013. Time scales of critical events around the Cretaceous-Paleogene boundary. Science 339, 684–687.
Riller, U., Poelchau, M.H., Rae, A.S., Schulte, F.M., Collins, G.S., Melosh, H.J., Grieve, R.A.F., Morgan, J.V., Gulick, S.P.S., Lofi, J., Diaw, A., McCall, N., Kring, D.A., 2018. Rock fluidization during peak-ring formation of large impact structures. Nature 562, 511.
Ríos, S., Salje, E.K., Zhang, M., Ewing, R.C, 2000. Amorphization in zircon: evidence for direct impact damage. J. Phys. Condens. Matter 12 (11), 2401.
Salje, E.K.H., Chrosch, J., Ewing, R.C., 1999. Is "metamictization" of zircon a phase transition? Am. Mineral. 84, 1107–1116.
Schlager, W., Buffler, R.T., Angstadt, D., Bowdler, J.L., Cotillon, P.H., Dallmeyer, R.D., Halley, R.B., Kinoshita, H., Magoon III, L.B., McNulty, C.L., Patton, J.W., Pisciotto, K.A., Premoli-Silva, I., Suarez, O.A., Testarmata, M.M., Tyson, R.V., Watkins, D.K., 1984. Deep sea drilling project, leg 77, southeastern Gulf of Mexico. GSA Bull. 95, 226–236.
Schmieder, M., Tohver, E., Jourdan, F., Denyszyn, S.W., Haines, P.W., 2015. Zircons from the Acraman impact melt rock (South Australia): shock metamorphism, U-Pb and $^{40}Ar/^{39}Ar$ systematics, and implications for the isotopic dating of impact events. Geochim. Cosmochim. Acta 161, 71–100.
Schmieder, M., Kring, D.A., Lapen, T.J., Gulick, S.P.S., Stockli, D.F., Rasmussen, C., Rae, A.S.P., Ferrière, L., Poelchau, M., Xiao, L., Wittmann, A., 2017. Sphene and TiO_2 assemblages in the Chicxulub peak ring: U-Pb systematics and implications for shock pressures, temperatures, and crater cooling. In: 80th Annual Meeting of the Meteoritical Society. 1987, Abstract No. 6134.
Schmieder, M., Shaulis, B.J., Lapen, T.J., Kring, D.A., 2018. U-Th-Pb systematics in zircon and apatite from the Chicxulub impact crater, Yucatán, Mexico. In: Geological Magazine. vol. 155. pp. 1330–1350.
Schulte, P., Alegret, L., Arenillas, I., Arz, J.A., Barton, P.J., Bown, P.R., Bralower, T.J., Christeson, G.L., Claeys, P., Cockell, C.S., Collins, G.S., Deutsch, A., Goldin, T.J., Goto, K., Grajales-Nishimura, J.M., Grieve, R.A.F., Gulick, S.P.S., Johnson, K.R., Kiessling, W., Koeberl, C., Kring, D.A., MacLeod, K.G., Matsui, T., Melosh, J., Montanari, A., Morgan, J.V., Neal, C.R., Nichols, D.J., Reimold, W.U., Robin, E., Salge, T., Speijer, R.P., Sweet, A.R., Urrutia-Fucugauchi, J., Vajda, V., Whalen, M.T., Willumsen, P.S., 2010. The Chicxulub asteroid impact and mass extinction at the Cretaceous-Paleogene boundary. Science 327, 1214–1218.
Schmieder, M., Shaulis, B.J., Lapen, T.J., Buchner, E., Kring, D.A., 2019. In situ U–Pb analysis of shocked zircon from the Charlevoix impact structure, Québec, Canada. Meteorit. Planet. Sci. https://doi.org/10.1111/maps.13315. (in press).
Silver, L.T., Deutsch, S., 1963. Uranium-lead isotopic variations in zircons: a case study. The Journal of Geology 71, 721–758.
Skipton, D.R., Schneider, D.A., McFarlane, C.R.M., St-Onge, M.R., Jackson, S.E., 2016. Multi-stage zircon and monazite growth revealed by depth profiling and in situ U-Pb geochronology: resolving the Paleoproterozoic tectonics of the Trans-Hudson Orogen on southeastern Baffin Island, Canada. Precambrian Res. 285, 272–298.
Sláma, J., Košler, J., Condon, D.J., Crowley, J.L., Gerdes, A., Hanchar, J.M., Horstwood, M.S.A., Morris, G.A., Nasdala, L., Norberg, N., Schaltegger, U., Schoene, B., Tubrett, M.N., Whitehouse, M.J., 2008. Plešovice zircon - a new natural reference material for U-Pb and Hf isotopic microanalysis. Chem. Geol. 249, 1–35.

Spencer, C.J., Kirkland, C.L., Taylor, R.J., 2016. Strategies towards statistically robust interpretations of in situ U–Pb zircon geochronology. Geosci. Front. 7, 581–589.
Sprain, C.J., Renne, P.R., Clemens, W.A., Wilson, G.P., 2018. Calibration of chron C29r: New high-precision geochronologic and paleomagnetic constraints from the Hell Creek region, Montana. Bulletin 130 (9-10), 1615–1644.
Stacey, J.S., Kramers, J.D., 1975. Approximation of terrestrial lead isotope evolution by a two-stage model. Earth Planet. Sci. Lett. 26, 207–221.
Steiner, M.B., Walker, J.D., 1996. Late Silurian plutons in Yucatan. Journal of Geophysical Research: Solid Earth 101, 17727–17735.
Schwarz, W.H., Breutmann, G., Schmitt, A.K., Trieloff, M., Ludwig, T., Hanel, M., Buchner, E., Schmieder, M., Pesonen, L.J., Moilanen, J., 2016. U/Pb dating of zircon from the Suvasvesi impact structures, Finland. 79th Annual Meeting of the Meteoritical Society, held 7–12 August, 2016 in Berlin, Germany. LPI Contribution No. 1921, id.6297.
Timms, N.E., Reddy, S.M., Healy, D., Nemchin, A.A., Grange, M.L., Pidgeon, R.T., Hart, R., 2012. Resolution of impact-related microstructures in lunar zircon: a shock-deformation mechanism map. Meteorit. Planet. Sci. 47, 120–141.
Timms, N.E., Erickson, T.M., Pearce, M.A., Cavosie, A.J., Schmieder, M., Tohver, E., Reddy, S.M., Zanetti, M.R., Nemchin, A.A., Wittmann, A., 2017. A pressure-temperature phase diagram for zircon at extreme conditions. Earth Sci. Rev. 165, 185–202.
Tohver, E., Lana, C., Cawood, P.A., Fletcher, I.R., Jourdan, F., Sherlock, S., Rasmussen, B., Trindade, R.I.F., Yokoyama, E., Souza, C.R., Marangoni, Y., 2012. Geochronological constraints on the age of a Permo-Triassic impact event: U-Pb and $^{40}Ar/^{39}Ar$ results for the 40 km Araguainha structure of central Brazil. Geochim. Cosmochim. Acta 86, 214–227.
Vermeesch, P.M., Morgan, J.V., 2008. Structural uplift beneath the Chicxulub impact structure. Journal of Geophysical Research Solid Earth 113, 1–10.
Weber, W.J., 1990. Radiation-induced defects and amorphization in zircon. J. Mater. Res. 5, 2687–2697.
Wendt, I., Carl, C., 1991. The statistical distribution of the mean squared weighted deviation. Chemical Geology: Isotope Geoscience Section 86, 275–285.
Wetherill, G.W., 1956. Discordant uranium-lead ages, I. EOS, Transactions American Geophysical Union 37, 320–326.
Wittmann, A., Kenkmann, T., Schmitt, R.T., Stöffler, D., 2006. Shock-metamorphosed zircon in terrestrial impact craters. Meteorit. Planet. Sci. 41, 433–454.
Woodhead, J.A., Rossman, G.R., Silver, L.T., 1991. The metamictization of zircon: Radiation dose-dependent structural characteristics. Am. Mineral. 76, 74–82.
Xiao, L., Zhao, J.W., Liu, H.S., Xiao, Z.Y., Morgan, J., Gulick, S., Kring, D., Claeys, P., Riller, U., the Expedition 364 Scientists, 2017. Ages and geochemistry of the basement granitoids of the Chicxulub impact crater: implications for peak ring formation. In: Lunar and Planetary Science Conference. 48, Abstract No. 1311.